Check for updates

Tensile Fiber Failure on High Strain Composites

Ajay Harihara Sharma [*]
University of Colorado, Boulder, CO 80303, USA

Seth Hill [†]
University of Colorado, Boulder, CO 80303, USA

Riley Perez [‡]
University of Colorado, Boulder, CO 80303, USA

TJ Rose [§]
Roccor, LLC, Longmont, CO 80503
University of Colorado, Boulder, CO 80303, USA

Francisco López Jiménez [¶]
University of Colorado, Boulder, CO 80303, USA

High Strain Composites are thin, carbon fiber reinforced polymer (CFRP) laminates that are designed to operate at strains higher than 1% under bending. Their failure properties are significantly different than those of thick laminates, including relatively high tensile strains and thickness dependence. We present a model to capture such behavior by taking into account the brittle nature of carbon fibers, quantified through an experimentally derived weakest link Weibull model. Instead of fully resolving the composite micromechanics, we analyze the composite as a combination of independent critical elements, so that failure of one of such elements results in catastrophic failure of the laminate. This paper presents the details of the model, as well as the experimental results used to characterize the fiber failure properties. The model is then applied to two different loading cases: pure tension as a simple example, and the more interesting case of bending with non-uniform curvature. After fitting to experiments, our model is able to capture the thickness dependence observed in Column Bending Test results.

I. Introduction

The use of carbon fiber composites is becoming increasingly widespread in deployable space structures. They are often used in strain energy based architectures (see Figure 1), which are an alternative to traditional designs that use complex mechanical elements. The stored strain energy allows for autonomous self-deployment, without the requirement of any external mechanical actuation. In order to improve the packaging ratio of these structures, recent designs are focusing on High Strain Composites (HSC), a class of composite materials designed to operate at strains higher than 1% in bending [1]. They are very thin laminates whose failure properties are significantly different from those of traditional composites. In addition to the high bending strains that they can sustain, two main differences are observed. First, when subjected to bending, HSCs fail in tension as opposed to failure due to microbuckling on the compression side [2]. This is attributed to the phenomenon known as shear stabilization [3–5], in which shear of the matrix between fibers in tension and compression is sufficiently high to increase the local loading necessary for the fibers to microbuckle.

---

[*]Graduate Student, Ann and H.J. Smead Department of Aerospace Engineering Sciences, University of Colorado, Boulder, AIAA Student Member

[†]Undergraduate Student,Ann and H.J. Smead Department of Aerospace Engineering Sciences, University of Colorado, Boulder

[‡]Undergraduate Student,Ann and H.J. Smead Department of Aerospace Engineering Sciences, University of Colorado, Boulder

[§]Sr. Mechanical Engineer, Roccor, LLC, Longmont; Graduate Student, Ann and H.J. Smead Department of Aerospace Engineering Sciences, University of Colorado, Boulder, AIAA Member.

[¶]Assistant Professor, Ann and H.J. Smead Department of Aerospace Engineering Sciences, University of Colorado, Boulder, AIAA Member.

Second, their failure under bending shows a dependency on the laminate thickness, with the failure strain increasing with decreasing thickness [6]. Several experimental and analytical studies have focused on the failure of HSCs [6–13], but the precise mechanics leading to their failure, particularly under bending is still not well understood.
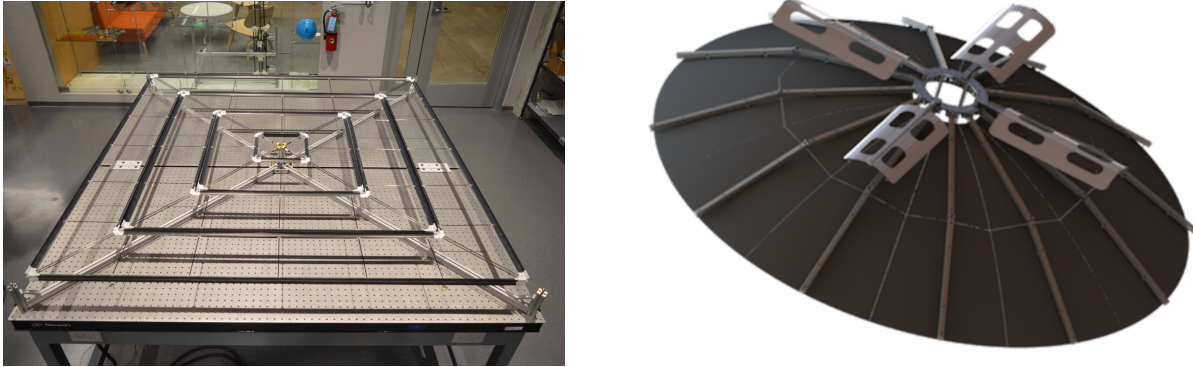
Fig. 1   Strain energy based elements used in deployable space structures : (a) spacecraft structure prototype [14]; and (b) deployable reflector [15]

We hypothesize that the reason for the thickness dependence of HSCs under bending, as well as the high strains observed in experiments, is due to the material properties of carbon fibers. Carbon fibers are brittle materials, and as such their failure is probabilistic in nature, determined by the presence of flaws. As a result, the failure of carbon fibers is volume-dependent and results in a wide range of possible tensile strengths. In the case of traditional composites, this effect of volume dependency of carbon fibers can be neglected, since at very large volumes of loaded fibers this variation becomes negligible. This is not the case for HSCs under bending, due to the small thickness and the concentrated region in which folding takes place. The goal of the present study is to incorporate the probabilistic nature of brittle failure in the modeling of HSCs by using a Weibull-type probability distribution to describe the behavior of such fibers.

The structure of this paper is as follows. Section II provides a background of the Weibull probabilistic distribution, which is used to describe the failure of carbon fibers in tension. Section III describes the testing campaign undertaken to characterize the failure parameters used in the Weibull-type failure description of IM7 fibers. In Section IV, we explain the failure model for a laminate made of IM7 fibers utilizing the parameters obtained from Section III. We do so with help of an example of a laminate subjected to tensile loading. We then apply this failure model to a laminate subjected to the Column Bending Test, which is the standard procedure to experimentally characterize the failure properties of HSCs under bending. We do so by utilizing the theory of elastica to predict strains and failure probabilities throughout the bent laminate.

II. Background

The brittleness of carbon fibers has been studied in depth [16–21]. It arises from internal flaws such as cracks, impurities, and misoriented crystallites. Brittle behavior is modeled using the 'Fiber Weak Link'(FWL) theory, which considers the fiber to be a chain of independent links, which will fail when the weakest of those links fails. Since the internal flaw is likely to be larger for a specimen of greater size, the fiber strength is gauge length dependent. As a result, composites made of carbon fibers exhibit size effects [21, 22]. In addition, the variation in internal flaws between different fibers is responsible for a considerable spread in the tensile strength of carbon fibers. This calls for a probabilistic approach to model their failure, and so the weakest link theory is often combined with a Weibull power law description of survival probability - also known as weakest link Weibull model [23].

Using the weakest link Weibull model, the failure probability of a fiber subjected to a given stress is given by the Weibull distribution:

$$P(\sigma, V) = 1 - \exp\left(-\frac{V}{V_0}\left(\frac{\sigma}{\sigma_0}\right)^m\right) . \tag{1}$$

Here, P is the probability of failure of a single fiber of volume V subjected to a uniform tensile stress σ. The two normalizing values, V_0 and σ_0 are reference values. Physically, V_0 is the volume of fiber used to experimentally characterize their failure, and σ_0 represents the reference stress for which a fiber of volume of V_0 has a probability of failure $P = 1 - \exp(-1) \approx 0.632$. The exponent m is the Weibull modulus; it is material dependent, and typically varies between 3 and 8 for carbon fibers [20, 24]. Physically, it represents the spread of possible failure stresses of the carbon fiber, thus accounting for the variation in flaw sizes for different fibers. Higher values of m indicate that defects are evenly distributed throughout the fibers, thereby resulting in most fibers failing at nearly the same stress. Lower values of m indicate that defects are fewer and more scattered, resulting in a large spread for the failure stress. This effect is shown in Figure 2, where for a value of $m = 100$, we can see that most fibers are likely to fail around $\sigma = \sigma_0$. As m decreases, the probable range of failure stresses for a fiber increases. Naito et. al [20] have shown that for polyacrylonitrile (PAN) and pitch based carbon fibers, an increase in tensile modulus and mean tensile strength is directly related to a decrease in Weibull modulus m.
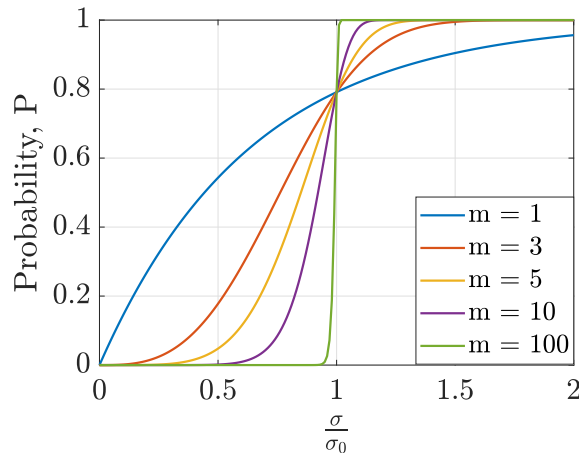
Fig. 2   Typical response of Weibull distribution function for different values of m.

Since carbon fibers form the backbone of CFRPs, it is essential to take the statistical distribution of the internal flaws into account to determine the failure of the laminates, especially for applications in which loading is concentrated in a small volume of the laminate. Several studies on CFRPs have focused on the application of Weibull probability distribution to evaluate failure of laminates [25–31]. Some of these models attempted to fit the Weibull parameters to evaluate the failure strength of laminates for a variety of applications such as investigating the effect of variation of strain rates and temperatures [26], evaluating hoop stress utilizing NOL ring tests [27], and failure due to fatigue [31] . Park *et al.* developed an analytical model [28] utilizing an improved continuum damage mechanics model incorporating five Weibull parameters. Others developed analytical models based on Weibull distribution for single fibers, and performed numerous experiments to validate their model [25, 29]. This study is one such extension of the Weibull probability model for single carbon fibers to evaluate the failure of a bent laminate subjected to the Column Bending Test.

III. Testing of IM7 Fibers to Evaluate Failure in Tension

In this study, we will focus on the failure properties of IM7 fibers, obtained through tensile testing on single filaments. IM7 is a high strength, intermediate modulus, PAN based aerospace grade carbon fiber; its manufacturer-provided properties [32] are detailed in Table 1 .

Tensile Strength (12K *tow*)	5654 MPa
Longitudinal Tensile Modulus, E_t	276 GPa
Tensile Failure Strain, ε_f	1.9 %
Filament Diameter, d_f	5.2 µm

3

Table 1 Properties of IM7 provided by the manufacturer - Hexcel [32].

The tests followed the ASTM D3379 standard (Standard Test Method for Tensile Strength and Young's Modulus for High-Modulus Single-Filament Materials, withdrawn, but with no replacement) [33]. A total of one hundred fibers were tested using an Instron 5969 with a 10 N load cell. The gauge length of each fiber was 30 mm and a uniform displacement rate of 1 mm/min was applied to each fiber until failure was observed. The stress was calculated using the nominal cross sectional area, calculated using the nominal, $d_f = 5.2\,\mu$m. The strain was directly obtained from the gauge length. The typical response of a fiber is shown in Figure 3. The initial flat region prior to 0 % strain corresponds to the release of slack in the fiber, which was introduced to avoid breakage while manipulating the sample prior to the test. The response shows a slight stiffening as the strain increases, followed by sudden failure.
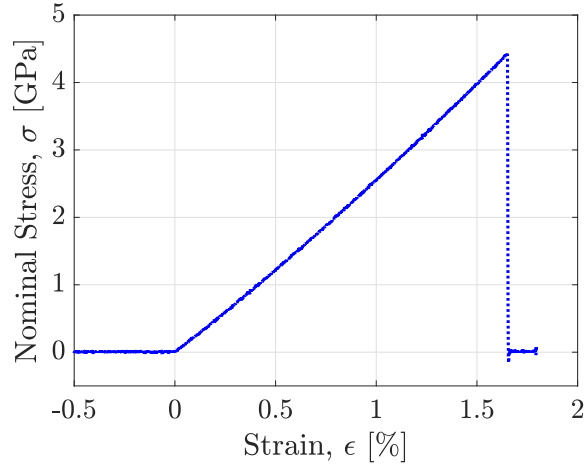
Fig. 3 Representative result of the tensile test of a single fiber.

The results of all tests performed are shown in Figure 4 as stress versus strain at failure. The material properties provided by Hexcel were also used to obtain the nominal axial stiffness given by $E_f \pi r_f^2$, which is represented by the dashed line in Figure 4. The deviations in stiffness are likely due to the different levels of stiffening of the fibers under tensile loading, as well as variations in the cross sectional area, since not all fibers have the same radius. For further computations, the strain at failure was the preferred value to characterize the failure of the fibers, since it is directly obtained from the gauge length and the test data, and does not rely on the cross sectional radius.

Rewriting the Weibull model in terms of strain yields:

$$P(\varepsilon, V) = 1 - \exp\left(-\frac{V}{V_0}\left(\frac{\varepsilon}{\varepsilon_0}\right)^{m'}\right) . \tag{2}$$

After basic rearrangement, we get:

$$\log\left(\log\frac{1}{1-P}\right) = m' \, \log\varepsilon - m' \, \log\varepsilon_0 . \tag{3}$$

This is a linear relationship of the form $y = \alpha x + \beta$, where $y = \log\left(\log\frac{1}{1-P}\right)$ and $x = \log\varepsilon$. The equation can be fit to the experimental results, yielding $\varepsilon_0 = \exp\left(-\frac{\beta}{m'}\right)$ and $m' = \alpha$. The probability of failure P_i for the i-th fiber strength was estimated [34] using:

4
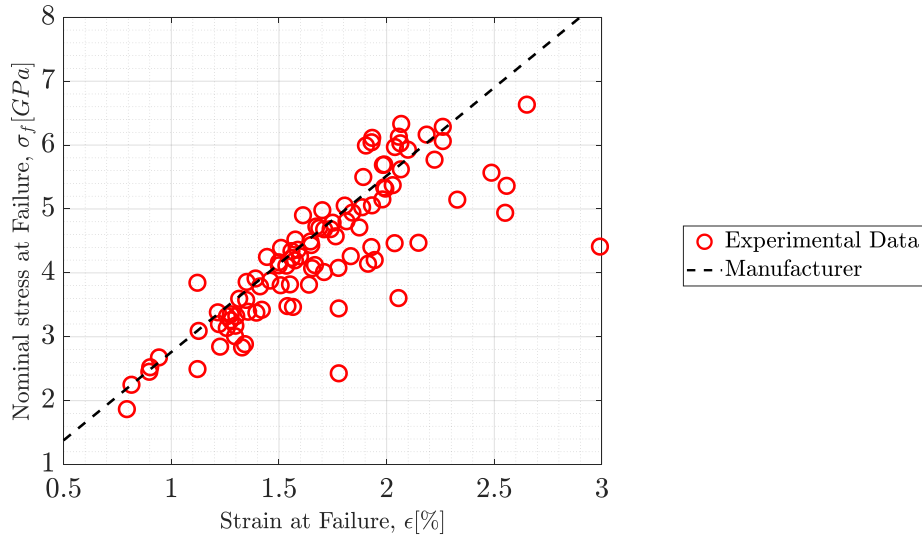
Fig. 4 Results of all tests conducted on IM7 fibers. The line shows the nominal axial stiffness, $E\,A$, calculated using values provided by the manufacturer.

$$P_i = \frac{i - 0.5}{N} \ . \tag{4}$$

The results are shown in Figure 5. For a reference volume of $V_0 = 6.37 \times 10^{-4}$ mm^3, we find $m' = 4.983$ and $\varepsilon_0 = 1.8402\%$.
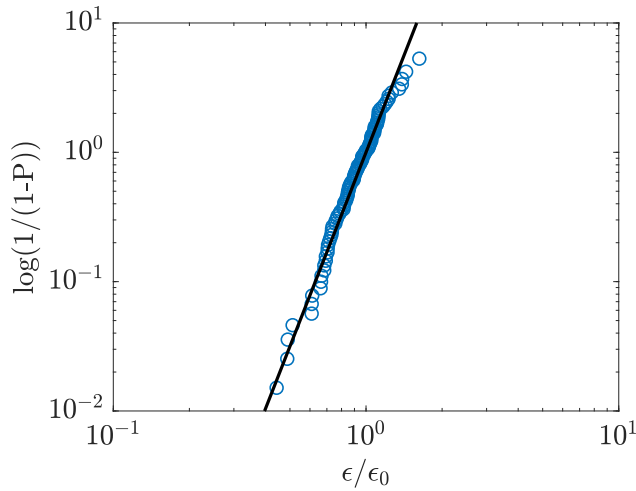
Fig. 5 Test results conducted on single IM7 fibers, expressed as a linear relationship.

IV. Analysis of Failure Probability for Bending of High Strain Composites

We now present a model that used the experimentally-obtained probabilistic description of single fiber failure to predict the failure of laminates. Our analysis is able to show dependence of failure strain on the variation in thickness for an HSC specimen under bending. It is important to emphasize that this analysis only deals with the probability of fiber

5

failure in tension; failure in compression, and in particular the suppression of microbuckling due to shear stabilization in very thin laminates needs to be addressed in parallel.

A. Failure Model

Previous models such as those of Ibnabdeljalil and Curtin [35] have considered it as a valid assumption to have the whole laminate follow the weakest link theory, *i.e.* once a sufficiently large element of the laminate fails, the crack propagates and the entire laminate fails. The main issue with this approach is determining the size of the characteristic element responsible for failure, as well as its failure probability as a function of the applied loading. As a first approximation, we assume that there exists a characteristic volume V^* that controls the weakest link theory for the laminate. We assume this characteristic volume V^* to be a cuboid of size $V^* = L_x L_y L_z$, where the direction z is aligned with the fibers. Henceforth, this cuboid would be referred to as the critical failure element. For this critical failure element, there will be a critical fiber failure density, ρ^*, which is the percentage of fibers that need to break within V^* to cause a catastrophic failure of the element, and therefore the laminate. Instead of modeling the micromechanics of the composite, as some of the studies referenced in Section II, here we follow a simplified approach in which we find these two parameters V^* and ρ^* by fitting to experimental values. As such, we avoid modeling the micromechanics at the fiber level, and we assume that the fibers are completely independent, *i.e.* breakage of one fiber has no effect on the fibers surrounding it. Instead, it is assumed that fitting the required values of V^* and ρ^* to experiments would take that effect into account in a phenomenological way. In reality, the failure of one fiber results in an increase in loading in the surrounding fibers [36–39], and so our value of ρ^* might not agree with the density of broken fibers in a real specimen at the point of failure [40].

To illustrate the above, let us consider a specimen subjected to tensile loading, *i.e.* a uniform strain state throughout the specimen. Consider the length, width, and thickness to be 30 mm, 25.4 mm and 1 mm respectively, with the fibers aligned with the length. This size is typical of an HSC subjected to the Column Bending Test. Since all the critical failure elements are subjected to the same strain, the probability of failure of each critical failure element, P_{f,V^*}, has the same value throughout the specimen. The probability of failure of the laminate, $P_{f,lam}$, in this case is given by:

$$P_{f,lam} = 1 - \left(P_{s,V^*}\right)^{n_{V^*inlam}} = 1 - \left(1 - P_{f,V^*}\right)^{n_{V^*inlam}} , \qquad (5)$$

where P_{s,V^*} represents the probability that the critical failure element survives and n_{V^*inlam} represents the number of critical failure elements in the laminate. For a specimen of volume V, the value n_{V^*inlam} is given by:

$$n_{V^*inlam} = \frac{V}{V^*} . \qquad (6)$$

Figure 6 shows a range of P_{f,V^*} that result in $P_{f,lam} > 0.5$ for this specific laminate under tension, as a function of n_{V^*inlam}. It was observed that holding V constant and varying V^* gave the same results as vice versa, and thus for this case, V was held constant while V^* was the parameter that varied. The dashed line represents a V^* value corresponding to $L_x = L_y = L_z = 25\,r_f$. Here, r_f is the radius of the fiber ($2.6\mu m$ for IM7 fibers as shown earlier in Table 1). Furthermore, let us assume $\rho^* = 0.03$. These specific values for V^* and ρ^* were obtained from two sources: literature and numerical experiments. Previous numerical studies of the micromechanics of uniaxial composites [38, 39] have shown that the influence of a broken fiber extends up to a distance of about $40\,r_f$. Although our model assumes the fibers to be independent, this particular region of increased stress concentration serves as a great reference value in conducting numerical experiments that were performed to obtain a range of acceptable values for the parameters V^* and ρ^*. The results are shown in Figure 9. Furthermore, it was seen that this particular set of parameters provided an excellent fit for an analysis considering the bending loading in a Column Bending Test, which will be discussed later in Section IV.B.
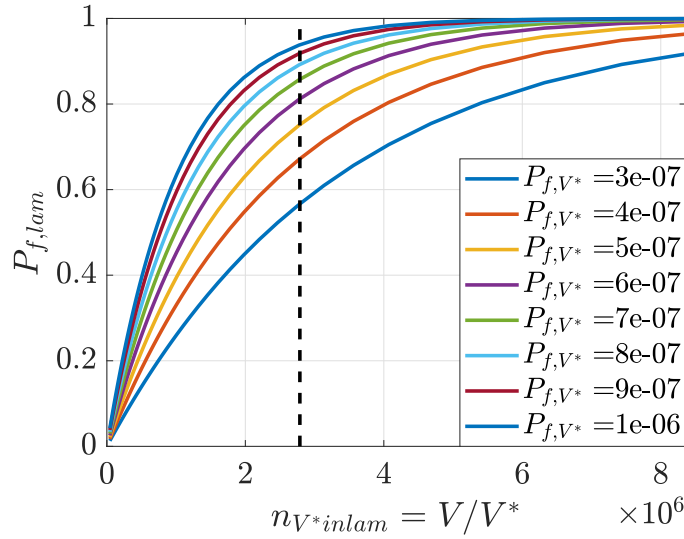
Fig. 6 Probability of failure of a laminate as a function of number of critical failure elements, for different values of the probability of failure of the element (P_{f,V^*}). We focus on the range of P_{f,V^*} that results in $P_{f,lam} > 0.5$ for a laminate under pure tensile loading of length, width and thickness equal 30 mm, 25.4 mm and 1 mm respectively. The dashed line represents a V^* value corresponding to $L_x = L_y = L_z = 25\, r_f$.

We now focus on calculating the value of the probability of failure of the critical element, P_{f,V^*}, as a function of the applied loading and the material parameters. In order to do so, we first evaluate the probability of failure of a single fiber of length L_z, that we denote as $P_{f,1fiber}$. This represents the probability that a fiber would fail in the region contained in a given critical failure element. To further simplify the analysis, we assume the strain to be constant within a given critical failure element. This assumption is true in the case of pure tension, and will lead to some error in more complex loading states. It results in $P_{f,1fiber}$ having the same value for all fibers within that element; a different element could have a different $P_{f,1fiber}$ depending on the loading state within the laminate. In order to evaluate $P_{f,1fiber}$, first let us consider a total of n_f fibers inside a critical failure element of characteristic volume V^*. Thus, we have:

$$n_f = \frac{L_x\, L_y\, V_f}{\pi\, r^2}\,, \tag{7}$$

where V_f represents the volume fraction of the fibers in the laminate and $L_x\, L_y$ represents the cross-sectional area of the critical failure element. The above equation for n_f assumes unidirectional fibers. For other architectures, similar calculations adjusting for the ratio of fibers aligned in a given direction could be obtained. If the given critical fiber failure density is ρ^*, we can obtain the critical number of fibers that need to fail to cause catastrophic failure of the critical element as $n_{f,cr} = n_f\, \rho^*$. For most of our calculations (unless specified), we round off both n_f and $n_{f,cr}$, since we need integer numbers for our analysis.

The probability of one fiber breaking in a given critical failure element under strain ε is given by Equation 8:

$$P_{f,1fiber} = 1 - \exp\left(-\frac{L_z \pi r^2}{V_0}\left(\frac{\epsilon}{\epsilon_0}\right)^{m'}\right)\,, \tag{8}$$

where $V = L_z \pi r^2$ represents the volume of the fiber and V_0, ε_0 and m' are the reference values obtained from single fiber testing, as described in Section III.

Figure 7 shows the probability of failure of one fiber, $P_{f,1fiber}$, under pure tensile loading, as a function of the applied strain, ε, and the length of the fiber, L_z. The scale on the right indicates logarithm (with base 10) of $P_{f,1fiber}$. The plot shows that the probability of failure increases not only with the applied strain, but also with the length

7

considered (L_z), since an increase in fiber volume results in a greater number of flaws. However, $P_{f,1fiber}$ is much more sensitive to strain compared to L_z, due to the exponent $m' = 4.983$ on the strain in Equation 8.
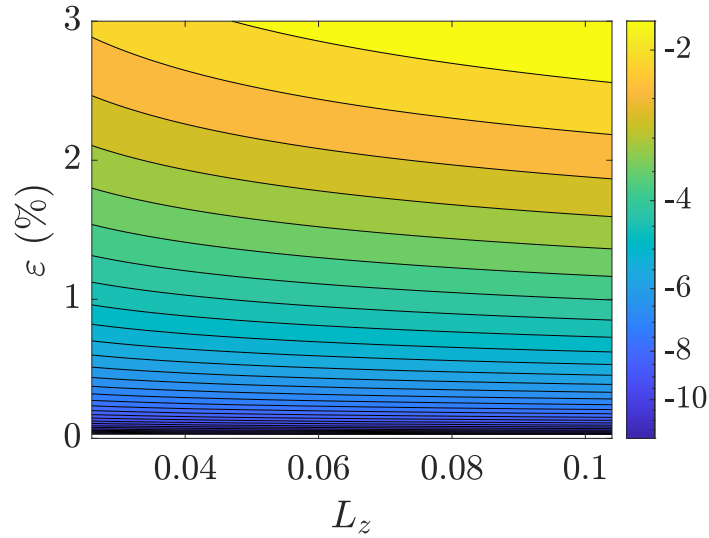
Fig. 7 Contour plot of probability of failure of one fiber, $P_{f,1fiber}$, as a function of strain in the fiber (ε) and length of the fiber, L_z. The scale indicates the logarithm (with base 10) of the probability of failure of one fiber.

Once we have obtained the probability of failure of a fiber, $P_{f,1fiber}$, we can evaluate the probability of failure of the critical failure element, P_{f,V^*}. In order to do so, assuming that the fibers are independent, we can represent the number of fibers failing by a binomial distribution function, $X \approx B(n, p)$, which models the probability $Pr(X = k)$ of having exactly k *successes* out of n total trials, each one with probability p. In our case, p is the probability of failure of a single fiber, $p = P_{f,1fiber}$, the number of trials is the number of fibers, $n = n_f$, and the k successes will be the failed fibers. The probability of failure of the critical element is therefore given by the probability of having at least $n_{f,cr}$ fibers failing, that is:

$$P_{f,V^*} = Pr(X \geq n_{f,cr}) = Pr(X = n_{f,cr}) + Pr(X = n_{f,cr} + 1) + Pr(X = n_{f,cr} + 2) + \ldots \tag{9}$$

However, solving Equation 9 directly is numerically expensive. As an alternative, we use the accumulative binomial, given by the regularized incomplete beta function, $I_x(a, b)$. In particular, the probability of a binomial $B(n, p)$ being less than k, is given by:

$$Pr(B(n, p) \leq k) = I_{1-p}(n - k, k + 1) . \tag{10}$$

This calculation is more efficient than Equation 9, and the incomplete beta function is available as a built-in function in most mathematical packages.

Equation 10 provides the probability of having *less* than a given number of failures. In that case, the volume V^* will survive if there are less than $n_{f,cr} - 1$ failures, and will fail in all other cases. This means, V^* will break only when we have more than $n_{f,cr}$ fibers failing, out of n_f total fibers, each one with a probability $P_{f1fiber}$. Mathematically, this can be represented as:

$$P_{s,V^*} = Pr\left(B(n_f, P_{f1fiber}) \leq n_{f,cr} - 1 \right) = I_{1-P_{f1fiber}}(n_f - n_{f,cr} + 1, n_{f,cr}) , \tag{11}$$

and so the probability of V^* failing is the opposite:

$$P_{f,V^*} = 1 - Pr\left(\quad B(n_f, P_{f1fiber}) \le n_{f,cr} - 1 \quad\right) = 1 - I_{1-P_{f1fiber}}(n_f - n_{f,cr} + 1, n_{f,cr}), \tag{12}$$

where $I_{1-P_{f1fiber}}(n_f - n_{f,cr} + 1, n_{f,cr})$ is the incomplete beta function, $I_x(a, b)$, with $x = 1 - P_{f1fiber}$, $a = n_f - n_{f,cr} + 1$ and $b = n_{f,cr}$.

To illustrate the method, let us consider again the same laminate under pure tension. Figure 8(a) and (b) show the predictions obtained from Equations 8 and 12, respectively. The range of values considered has been chosen so that the analysis yields the same range probability of failure of the laminate shown in Figure 6. The dashed line in Figure 8 corresponds to a total number of fibers within the critical failure element $n_f = 119$, obtained by substituting our reference parameter $L_x = L_y = L_z = 25\,r_f$ in Eqn. 7. The figures are useful to identify that values in the range of $P_{f,V^*} \in \left[3 \times 10^{-7}, 1 \times 10^{-6}\right]$ and $P_{f,1fiber} \in \left[2.4 \times 10^{-4}, 4 \times 10^{-4}\right]$, yield the desired range of $P_{f,lam} > 0.5$ for the failure of the laminate. It is important to clarify that to obtain these results, the critical numbers of fibers $n_{f,cr}$ has not been rounded off to an integer value in order to obtain a smooth plot.
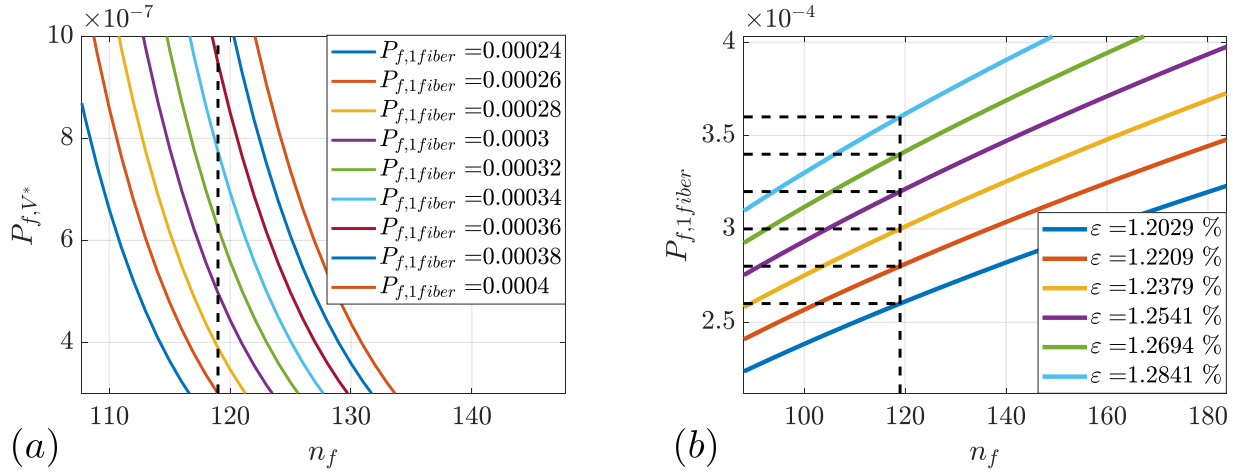
Fig. 8 (a) Probability of failure P_{f,V^*} of the same critical failure element considered in Figure 6, as a function of number of fibers within the element n_f, for different values of $P_{f,1fiber}$, and (b) Probability of failure of one fiber $P_{f,1fiber}$ as a function of number of fibers within the failure element n_f, for different values of strain in the fiber. The probability of failure of one fiber $P_{f,1fiber}$ as well as the strain values in the two plots yield values of P_{f,V^*} in a range that result in $P_{f,lam} > 0.5$ for a laminate of length, width, and thickness equal 30 mm, 25.4 mm and 1 mm respectively.

It is important to highlight that the failure strain in tension predicted by the model for the reference parameters $L_x = L_y = L_z = 25\,r_f$ and $\rho^* = 0.03$ lies between 1.2% and 1.3%, which is lower than the manufacturer specified strain of 1.9%. However, the previous values correspond to an example with a given set of values of the two key parameters, V^* and ρ^*, which have been fitted to CBT data, as will be explained in Section IV.B. Figure 9 shows a more thorough exploration of the design space, in the form of a contour plot of the applied strain ε [%] necessary to achieve a probability of failure of the laminate $P_{f,lam} = 90\%$, for different values of V^* and ρ^*. The saw-like phenomenon observed in the plot is due to the discrete nature of the model, which relies on integer numbers for both n_f and $n_{f,cr}$. The results obtained from this plot help illustrate that there are several values of the two input parameters(V^* and ρ^*) that result in the same required applied strain, for the case of pure tension. The model will require calibration taking into account data from a wide range of geometries and loading cases before it can be used for the analysis of a structure under realistic conditions.
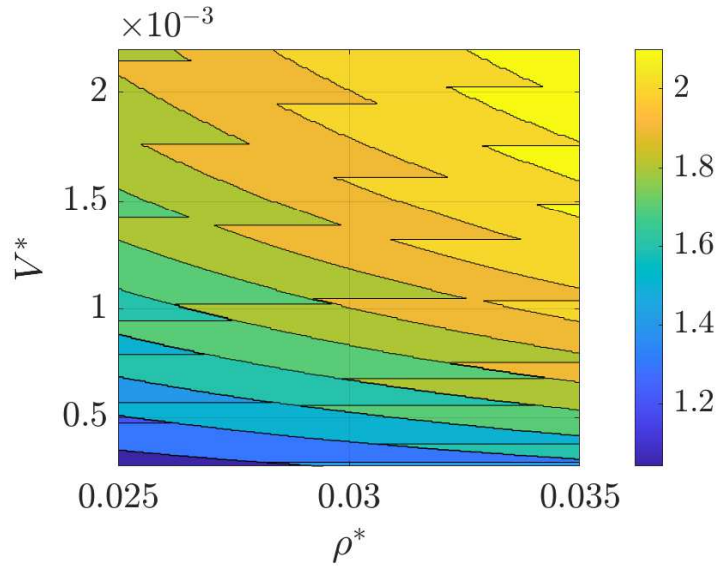
Fig. 9 Contour plot of failure strain, for a laminate subjected to uniform tensile loading, predicted by the model as a function of the two parameters V^* and ρ^*. The specimen has a length, width and thickness of 30 mm, 25.4 mm and 1 mm respectively. The scale indicates the failure strain predicted by the model for a given set of parameters V^* and ρ^* to achieve $P_{f,lam} = 90\%$.

B. Application to a Column Bending Test Specimen

We now apply the model to a specimen in the Column Bending Test. In this case, the strain at every point will be equal to:

$$\varepsilon = \kappa z \,, \tag{13}$$

where κ is the curvature of the specimen, and z is the distance to the neutral axis, which will be assumed to remain at the geometric centroid of the laminate.

Since the curvature in CBT specimens is not constant along the arclength, it is necessary to account for its variation to obtain an accurate value for the probability of failure. In order to do so, the behavior of the coupon has been modeled using Euler's theory of elastica, which is a large deformation theory that is able to capture the large scale deflection of structural elements.

Assuming that the specimen is inextensible, we use the constitutive relationship between moment and curvature given by:

$$M(s) = EI\kappa(s) = EI\beta'(s) \tag{14}$$

where $M(s)$ represents the bending moment at every point along the arclength parameter s, E represents the Young's modulus of the HSC specimen, I represents the area moment of inertia of the bent specimen, $\kappa(s)$ is the curvature at every point along the arclength, and β represents the angle between a vector tangent to the coupon and the vertical axis at every point along the curve. We will assume that both E and I are constant, since it has been shown previously [8] that variation of bending stiffness due to fiber non-linearity does not have much of an impact on the curvature. Considering l to be the length of each rigid arm used in CBT, the differential equations for the position co-ordinates $x(s)$ and $y(s)$ can be given in terms of the angle $\beta(s)$ as:

10
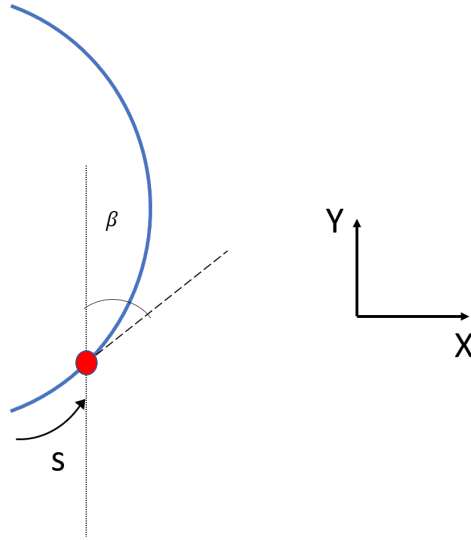
Fig. 10 Representation of the elastica. Here, s is the arclength parameter and β represents the angle between the a vector tangent to the coupon and the vertical axis at every point along the curve.

$$\frac{dx}{ds} = \sin\beta\,, \tag{15}$$

$$\frac{dy}{ds} = \cos\beta\,. \tag{16}$$

For the geometry of the problem, the bending moment can be expressed as:

$$EI\frac{d\beta}{ds} = M = P\left(x + l\sin\frac{\phi}{2}\right) \tag{17}$$

where x is the horizontal distance to the loading axis, P is the external load, and ϕ is the angle of the rigid arm with the vertical axis.

The above equations have been integrated numerically in Matlab using the 'ode45' function. For this problem, the boundary conditions are $\theta_{midpoint} = 0$, $x_0 = 0$ and $y_0 = 0$. A shooting algorithm has been implemented here which helps evaluate the value of the applied loading necessary to satisfy the condition $\theta_{midpoint} = 0$. This boundary condition was used because no other condition can be expressed as an initial boundary condition. The numerical integration provides the shape of the specimen as well as the distribution of curvature across the arclength, $\kappa(s)$ for each applied vertical displacement δ of the testing machine. The bending moment can then be calculated as either $Px(s)$ or $EI\kappa(s)$.

Once the curvature is calculated, the representative strain of each critical element is calculated using Equation 13. Since now the strain is different at each point, the values of the probability of failure of the critical elements, P_{f,V^*}, will also be different, and the probability of failure of the laminate is calculated as:

$$P_{f,lam} = 1 - \prod_{n_{V^*-in-lam}} P_{s,V^*} = 1 - \prod_{n_{V^*-in-lam}} (1 - P_{f,V^*}) \tag{18}$$

which only takes into account the elements on the tension side.

Figure 11 shows the results from three representative values of thickness t and freelength l_s as probability of failure of the laminate versus nominal bending strain on the laminate, obtained using the maximum curvature of the elastica at

11

each point of the test. The parameters used here for the model are the same as before (*i.e.*, $L_x = L_y = L_z = 25 \, r_f$ and $\rho^* = 0.03$). The dashed vertical line represents the manufacturer specified failure strain for IM-7 fibers. The results show that for the same nominal strain, the probabilities of failure are very different and there is a clear dependence of thickness and the freelength on the probability of failure. For the same value of nominal strain, specimens having lower thickness and a lower free length have a lower probability of failure.
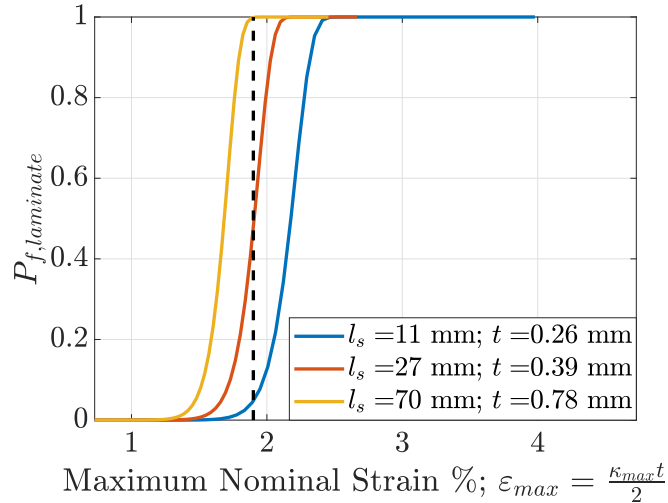
Fig. 11 Probability of failure of the laminate as a function of maximum nominal strain obtained from the elastica. The straight dashed line corresponds to the manufacturer specified failure strain of 1.9 %. The parameters utilized in the model are $L_x = L_y = L_z = 25 \, r_f$ and $\rho^* = 0.03$.

Two important differences between these results and the case for tension must be highlighted. First, since the strain is not constant through V^*, the value at the centroid of the element is used as a representative value. Second, High Strain Composites tested using the Column Bending Test method often have very small thickness, well below one millimeter. In such cases, the size of the critical failure element ($L_x = L_y = L_z = 25r_f$) is of the same order of magnitude as the thickness dimension of the portion under tension, and so the number of elements across the thickness is very small (e.g. a specimen of 0.5 mm thickness would have approximately 4 elements on the tensile side).

Finally, Figure 12 compares our model with experimental CBT data. The dots correspond to experiments using HSC laminates made of IM7 fibers and PMT-F7 matrix. The values are presented as nominal strain, $\frac{\kappa t}{2}$, versus the thickness of the laminate. The error bars indicate variation in both variables. The thinnest samples, with $t \approx 141 \, \mu m$, did not break; the reported curvature represents the maximum curvature applied during the test. The failure curvatures were obtained using image processing of test images, as well as results from the closed form solution commonly used to model the Column Bending Test [8]. The model uses the same parameters as in previous plots, *i.e.* $L_x = L_y = L_z = 25 \, r_f$ and $\rho^* = 0.03$. The two prediction curves correspond to the nominal strain that results in a probability of failure of the laminate of $P_{f,lam} = 80\%$ and $P_{f,lam} = 95\%$. We can see that, despite the strong simplification and assumptions, the proposed probabilistic model is able to capture the thickness dependency of failure strain for an HSC.
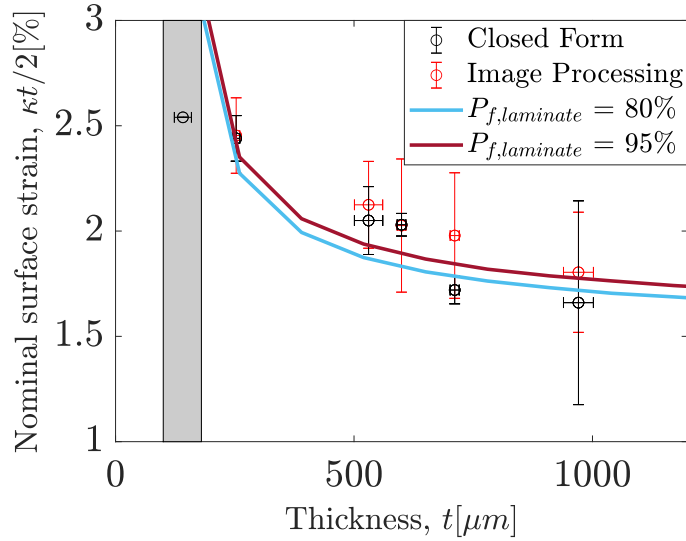
Fig. 12 Results of Column Bending Tests conducted on High Strain Composites of different thicknesses. The gray region represents test data of the thinnest HSCs with $t \approx 141\,\mu$m, which did not break when subjected to the maximum possible extension of the testing machine. The proposed model is able to capture the thickness dependence of failure strain utilizing the set of parameters $L_x = L_y = L_z = 25\,r_f$ and $\rho^* = 0.03$.

Conclusions and Future Work

We have presented a model that incorporates the probabilistic nature of the failure of carbon fibers to capture some key elements of the failure of High Strain Composites. However, the current iteration of the model rests on several important assumptions, whose validity need to be addressed.

First, we have neglected the non-linearity of the fibers, which was noticeable in Figure 3. A constitutive model that takes into account the nonlinearity [41, 42] will result in a shift of the neutral axis, and changes in the strain at the critical elements. Second, we have very few critical failure elements across the thickness. Thus, evaluating the failure strain at the midpoint of the critical failure element, and considering it to be a constant value throughout the thickness dimension of that element, is a very strong assumption. This is true especially for very thin HSCs, since they have a rapidly decreasing strain gradient across the thickness. The validity of this assumption needs to be verified through parametric studies and further comparison with experiments. Finally, different sets of values of V^* and ρ^* can result in the same macroscopic failure properties. Figure 13 presents the same experimental results and predictions as Fig. 12, adding a new prediction obtained with $L_x = L_y = L_z = 30\,r_f$ and $\rho^* = 0.025$, which provides a very similar prediction. This was also apparent in the tension predictions presented in Fig. 7.

13
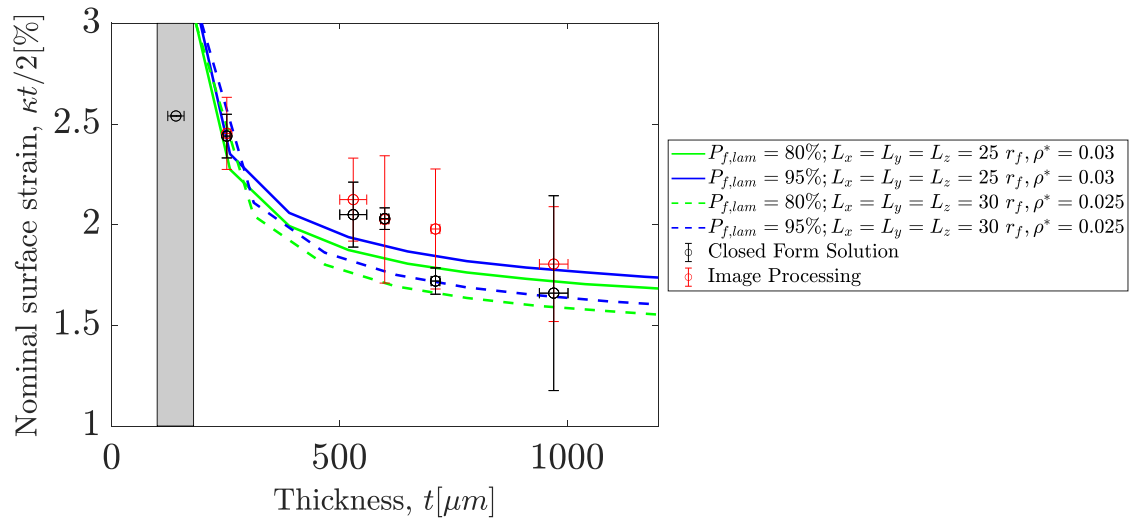
Fig. 13 Results of Column Bending Tests conducted on High Strain Composites of different thicknesses. The gray region represents test data of the thinnest HSCs with $t \approx 141 \, \mu$m, which did not break when subjected to the maximum possible extension of the testing machine. The predictions correspond to two different set of values of V^* and ρ^*.

It is clear that, in order to obtain reliable values of the two model parameters, it will be necessary to obtain additional experimental data, and fit the model to different geometries and loading conditions. Furthermore, the critical element V^* does not need to have equal dimensions. In particular, the length along the fiber direction, L_z, can be different from the cross sectional dimensions, $L_x = L_y$. While L_z influences the probability of failure of a single fiber, L_x and L_y determine the number of fibers in V^*, and so decoupling them will in practice add an additional parameter to the model. We are currently in the process of providing new experimental results, such as more CBT cases, and tensile loading with different thicknesses and gauge lengths.

Acknowledgments

14

References

[1] Murphey, T. W., Francis, W., Davis, B., and Mejia-Ariza, J. M., "High strain composites," *2nd AIAA Spacecraft Structures Conference*, 2015, p. 0942.

[2] Marissen, R., and Brouwer, H., "The significance of fibre microbuckling for the flexural strength of a composite," *Composites science and technology*, Vol. 59, No. 3, 1999, pp. 327–330.

[3] Drapier, S., Grandidier, J.-C., and Potier-Ferry, M., "Towards a numerical model of the compressive strength for long fibre composites," *European Journal of Mechanics-A/Solids*, Vol. 18, No. 1, 1999, pp. 69–92.

[4] Murphey, T., Meink, T., and Mikulas, M., "Some micromechanics considerations of the folding of rigidizable composite materials," *19th AIAA Applied Aerodynamics Conference*, 2001, p. 1418.

[5] Francis, W., Lake, M., Schultz, M., Campbell, D., Dunn, M., and Qi, H. J., "Elastic memory composite microbuckling mechanics: closed-form model with empirical correlation," *48th AIAA/ASME/ASCE/AHS/ASC Structures, Structural Dynamics, and Materials Conference*, 2007, p. 2164.

[6] Rose, T., Sharma, A., Seamone, A., López Jiménez, F., and Murphey, T., "Carbon Unidirectional Composite Flexure Strength Dependence on Laminate Thickness," *Proceedings of the American Society for Composites—Thirty-third Technical Conference*, 2018.

[7] Murphey, T. W., Peterson, M. E., and Grigoriev, M. M., "Four point bending of thin unidirectional composite laminas," *54th AIAA/ASME/ASCE/AHS/ASC Structures, Structural Dynamics, and Materials Conference*, 2013, p. 1668.

[8] Sharma, A. H., Rose, T., Seamone, A., Murphey, T. W., and López Jiménez, F., "Analysis of the Column Bending Test for Large Curvature Bending of High Strain Composites," *AIAA Scitech 2019 Forum*, 2019.

[9] Sanford, G., Biskner, A., and Murphey, T., "Large strain behavior of thin unidirectional composite flexures," *51st AIAA/ASME/ASCE/AHS/ASC Structures, Structural Dynamics, and Materials Conference 18th AIAA/ASME/AHS Adaptive Structures Conference 12th*, 2010, p. 2698.

[10] López Jiménez, F., and Pellegrino, S., "Folding of fiber composites with a hyperelastic matrix," *International Journal of Solids and Structures*, Vol. 49, No. 3-4, 2012, pp. 395–407.

[11] Medina, K., Rose, T., and Murphey, T. W., "Initial Investigation of Time Dependency on Failure Curvatures of FlexLam High Strain Composites," *Proceedings of the American Society for Composites—Thirty-second Technical Conference*, 2017.

[12] Fernandez, J. M., and Murphey, T. W., "A Simple Test Method for Large Deformation Bending of Thin High Strain Composite Flexures," *2018 AIAA Spacecraft Structures Conference*, 2018, p. 0942.

[13] Herrmann, K. M., *An Investigation of a Vertical Test Method for Large Deformation Bending of High Strain Composite Laminates*, 2017.

[14] Gdoutos, E., Leclerc, C., Royer, F., Türk, D. A., and Pellegrino, S., "Ultralight spacecraft structure prototype," *AIAA Scitech 2019 Forum*, 2019, p. 1749.

[15] Footdale, J. N., Peterson, M., and Griffee, J. C., "Flexible Composite Shell Design for the MARCO Deployable Reflector," *AIAA Scitech 2019 Forum*, 2019, p. 0756.

[16] Pickering, K., and Murray, T., "Weak link scaling analysis of high-strength carbon fibre," *Composites Part A: Applied Science and Manufacturing*, Vol. 30, No. 8, 1999, pp. 1017–1021.

[17] Moreton, R., and Watt, W., "Tensile strengths of carbon fibres," *Nature*, Vol. 247, No. 5440, 1974, p. 360.

[18] Johnson, D., "Structure-property relationships in carbon fibres," *Journal of Physics D: Applied Physics*, Vol. 20, No. 3, 1987, p. 286.

[19] Burnay, S., and Sharp, J., "Defect structure of PAN-based carbon fibres," *Journal of Microscopy*, Vol. 97, No. 1-2, 1973, pp. 153–163.

[20] Naito, K., Tanaka, Y., Yang, J.-M., and Kagawa, Y., "Tensile properties of ultrahigh strength PAN-based, ultrahigh modulus pitch-based and high ductility pitch-based carbon fibers," *Carbon*, Vol. 46, No. 2, 2008, pp. 189–195.

[21] Tagawa, T., and Miyata, T., "Size effect on tensile strength of carbon fibers," *Materials Science and Engineering: A*, Vol. 238, No. 2, 1997, pp. 336–342.

[22] Wisnom, M., "Size effects in the testing of fibre-composite materials," *Composites Science and Technology*, Vol. 59, No. 13, 1999, pp. 1937–1957.

[23] Zok, F. W., "On weakest link theory and Weibull statistics," *Journal of the American Ceramic Society*, Vol. 100, No. 4, 2017, pp. 1265–1268.

[24] Bader, M. G., Pickering, K. L., Buxton, A., Rezaifard, A., and Smith, P. A., "Failure micromechanisms in continuous carbon-fibre/epoxy-resin composites," *Composites science and technology*, Vol. 48, No. 1-4, 1993, pp. 135–142.

[25] Manders, P. W., and Bader, M., "The strength of hybrid glass/carbon fibre composites," *Journal of materials science*, Vol. 16, No. 8, 1981, pp. 2246–2256.

[26] Ou, Y., Zhu, D., Zhang, H., Yao, Y., Mobasher, B., and Huang, L., "Mechanical properties and failure characteristics of CFRP under intermediate strain rates and varying temperatures," *Composites Part B: Engineering*, Vol. 95, 2016, pp. 123–136.

[27] Vardhan, A. V., Charan, V. S. S., Raj, S., Hussaini, S., and Rao, G., "Failure prediction of CFRP composites using Weibull analysis," *AIP Conference Proceedings*, Vol. 2057, AIP Publishing, 2019, p. 020014.

[28] Park, K. J., Kang, H.-j., Choi, I.-H., Shin, S., and Kim, S. J., "Progressive failure analysis of carbon-fiber reinforced polymer (CFRP) laminates using combined material nonlinear elasticity and continuum damage mechanics based on treatment of coupon test," *Journal of Composite Materials*, Vol. 50, No. 11, 2016, pp. 1431–1455.

[29] Okabe, T., Ishii, K., Nishikawa, M., and Takeda, N., "Prediction of tensile strength of unidirectional CFRP composites," *Advanced Composite Materials*, Vol. 19, No. 3, 2010, pp. 229–241.

[30] Okabe, T., and Takeda, N., "Size effect on tensile strength of unidirectional CFRP composites—experiment and simulation," *Composites Science and Technology*, Vol. 62, No. 15, 2002, pp. 2053–2064.

[31] Harris, B., Gathercole, N., Lee, J., Reiter, H., and Adam, T., "Life–prediction for constant–stress fatigue in carbon–fibre composites," *Philosophical Transactions of the Royal Society of London. Series A: Mathematical, Physical and Engineering Sciences*, Vol. 355, No. 1727, 1997, pp. 1259–1294.

[32] *HexTow® IM7 Carbon Fiber Datasheet*, Hexcel, 2019.

[33] ASTM, A., et al., "Standard Test Method for Tensile Strength and Young's Modulus for High-Modulus Single-Filament Materials," , 1989.

[34] Trustrum, K., and Jayatilaka, A. D. S., "On estimating the Weibull modulus for a brittle material," *Journal of Materials Science*, Vol. 14, No. 5, 1979, pp. 1080–1084.

[35] Ibnabdeljalil, M., and Curtin, W. A., "Strength and reliability of fiber-reinforced composites: localized load-sharing and associated size effects," *International Journal of Solids and Structures*, Vol. 34, No. 21, 1997, pp. 2649–2668.

[36] Phoenix, S., and Raj, R., "Overview no. 100 Scalings in fracture probabilities for a brittle matrix fiber composite," *Acta metallurgica et materialia*, Vol. 40, No. 11, 1992, pp. 2813–2828.

[37] Curtin, W. A., and Takeda, N., "Tensile strength of fiber-reinforced composites: I. Model and effects of local fiber geometry," *Journal of composite materials*, Vol. 32, No. 22, 1998, pp. 2042–2059.

[38] St-Pierre, L., Martorell, N. J., and Pinho, S. T., "Stress redistribution around clusters of broken fibres in a composite," *Composite Structures*, Vol. 168, 2017, pp. 226–233.

[39] Tavares, R. P., Otero, F., Turon, A., and Camanho, P. P., "Effective simulation of the mechanics of longitudinal tensile failure of unidirectional polymer composites," *International Journal of Fracture*, Vol. 208, No. 1-2, 2017, pp. 269–285.

[40] Scott, A., Sinclair, I., Spearing, S., Thionnet, A., and Bunsell, A. R., "Damage accumulation in a carbon/epoxy composite: comparison between a multiscale model and computed tomography experimental results," *Composites Part A: Applied Science and Manufacturing*, Vol. 43, No. 9, 2012, pp. 1514–1522.

[41] Ishikawa, T., Matsushima, M., and Hayashi, Y., "Hardening non-linear behaviour in longitudinal tension of unidirectional carbon composites," *Journal of materials science*, Vol. 20, No. 11, 1985, pp. 4075–4083.

[42] Northolt, M., Veldhuizen, L., and Jansen, H., "Tensile deformation of carbon fibers and the relationship with the modulus for shear between the basal planes," *Carbon*, Vol. 29, No. 8, 1991, pp. 1267–1279.